Article

pubs.acs.org/Biomac

Positron Emission Tomography Based Analysis of Long-Circulating Cross-Linked Triblock Polymeric Micelles in a U87MG Mouse Xenograft Model and Comparison of DOTA and CB-TE2A as Chelators of Copper-64

Andreas I. Jensen,[†,‡] Tina Binderup,[§] Pramod Kumar EK,[‡] Andreas Kjær,[§] Palle H. Rasmussen,[†] and Thomas L. Andresen*[,‡]

[†]The Hevesy Laboratory, DTU Nutech, Technical University of Denmark, Roskilde, Denmark

[‡]Department of Micro- and Nanotechnology, Center for Nanomedicine and Theranostics, DTU Nanotech, Technical University of Denmark, Building 423, 2800 Lyngby, Denmark

[§]Cluster for Molecular Imaging and Department of Clinical Physiology, Nuclear Medicine, and PET, Rigshospitalet, University of Copenhagen, Copenhagen, Denmark

Supporting Information

ABSTRACT: Copolymers of ABC-type (PEG-PHEMA-PCMA) architecture were prepared by atom transfer radical polymerization and formulated as micelles with functionalizable primary alcohols in the shell-region (PHEMA-block) to which the metal-ion chelators DOTA or CB-TE2A were conjugated. Using this micelle system we compared the in vivo stabilities of DOTA and CB-TE2A as chelators of ^{64}Cu in micelle nanoparticles. The coumarin polymer (PCMA-block) micelle core was cross-linked by UV irradiation at 2 W/cm^2 for 30 min. The cross-linked micelles were labeled with ^{64}Cu at room temperature for 2 h (DOTA) or 80 °C for 3 h (CB-TE2A), giving labeling efficiencies of 60−76% (DOTA) and 40−47% (CB-TE2A). ^{64}Cu-micelles were injected into tumor-bearing mice (8 mg/kg) and PET/CT scans were carried out at 1, 22, and 46 h postinjection. The micelles showed good blood stability ($T_{1/2}$: 20−26 h) and tumor uptake that was comparable with other nanoparticle systems. The DOTA micelles showed a biodistribution similar to the CB-TE2A micelles and the tumor uptake was comparable for both micelle types at 1 h (1.9% ID/g) and 22 h (3.9% ID/g) but diverged at 46 h with 3.6% ID/g (DOTA) and 4.9% ID/g (CB-TE2A). On the basis of our data, we conclude that cross-linked PEG-PHEMA-PCMA micelles have long circulating properties resulting in tumor accumulation and that DOTA and CB-TE2A ^{64}Cu-chelates show similar in vivo stability for the studied micelle system.

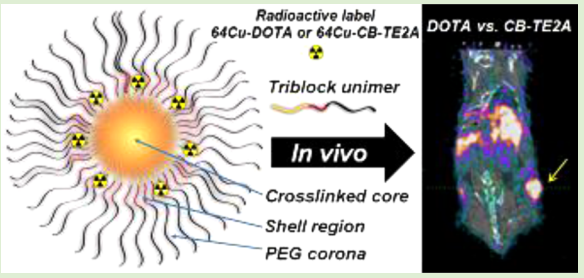

INTRODUCTION

Long circulating nanoparticles are able to passively target tumor tissue through the EPR-effect,[1] which makes them useful as drug delivery vehicles in cancer therapy. In recent years, there has been a growing interest in the possible use of nanoparticles as therapeutic and diagnostic radiopharmaceuticals for tumor therapy and imaging. However, poor tumor penetration may hamper accumulation in cancerous tissue[2] and cause nanoparticles to deposit in the tumor periphery.[3] Contributing to poor penetration is the dense extracellular matrix (ECM) present in tumors.[4] Recent research has shown that nanoparticles smaller than 50 nm may exhibit superior tumor accumulation in poorly vascularized tumors,[5,6] possibly because of increased diffusion capability in the ECM.[7] For this reason, the interest in small nanoparticles, such as polymeric micelles (PMs), is currently high.[8]

Imaging is a powerful tool for investigating and improving the *in vivo* properties of nanoparticles, particularly positron emission tomography (PET) imaging. PET relies on the coincidence detection of antiparallel photons emitted by annihilation of positrons with electrons. Compared with single photon emission computed tomography (SPECT), PET is a truly quantitative technique that in addition offers superior sensitivity and spatial resolution.[9,10] Thus, methods for labeling of nanoparticles with radionuclides that allow for PET imaging is attracting increasing attention.[8,11,12] ^{64}Cu is a particularly popular isotope due to its 12.7 h half-life allowing PET scans for up to 48 h after injection, which is sufficient to study the biodistribution of long-circulating nanoparticles.

In order to conjugate ^{64}Cu to nanoparticles, chelators are used. Traditionally, DOTA and TETA have been popular choices as they are widely available as bifunctional chelators and can be efficiently labeled at ambient temperature.[13,14] However, the in vivo stability of these chelators is widely questioned.[15,16]

Received: December 18, 2013
Revised: March 15, 2014
Published: March 19, 2014

^{64}Cu has been shown to escape from DOTA through transchelation to superoxide dismutase in the liver.[17−19] In addition, after injection of ^{64}Cu bound to DOTA and TETA, ^{64}Cu was shown to associate with blood proteins[18] and ^{64}Cu bound to a DOTA-conjugated peptide caused more liver accumulation than a different radiolabel (^{86}Y), which was indicative of transchelation.[20] Despite these findings, DOTA remains in widespread use in clinical imaging.[21] CB-TE2A is a chelator that has been championed as providing both improved thermodynamic and kinetic stability over TETA and DOTA.[22−24] However, labeling of CB-TE2A with $^{64}Cu^{2+}$ requires relatively harsh conditions, such as 1−2 h at 95 °C (pH = 8) for labeling yields of ≥95%[13,25] or 1 h at 85 °C (pH = 5.5) for labeling of 96%.[26] This is undesirable when labeling proteins, liposomes, or other structures labile to high temperatures, but for thermostable structures CB-TE2A provides a very sturdy chelate. When conjugating chelators to nanoparticles, the location of the chelator may have importance. When chelators are placed near the surface of liposomes, protected by the PEG-layer, lower liver, and spleen accumulation has been shown to occur in comparison with placement at the distal end of PEG.[26] Fonge et al. concluded that the employed chelator has significant effects on nanoparticle pharmacokinetics, beyond what can be explained by complexation stability.[27] They used chelators that were placed on the distal end of PEG. This suggests that the chemical structure of chelators may influence pharmacokinetics, when they can come into contact with the biological environment in the bloodstream. In addition, studies of proteins have concluded that the position and chemical structure of the chelators used may influence pharmacokinetics.[28−30]

For these reasons, we designed small (30−40 nm) core−shell−corona (ABC) triblock PMs featuring primary alcohols in a functionalizable shell-region (Figure 1). In order to compare

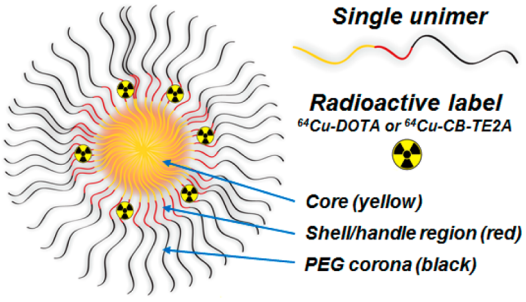

Figure 1. Cartoon of a radiolabeled ABC-type triblock polymeric micelle. In this study was used PEG-PHEMA-PCMA unimers. The single unimer consists of (1) a hydrophobic 4-methylcoumarin-containing monomer (PCMA, yellow), (2) a functionalizable shell-region containing an alcohol (PHEMA, red), and (3) a hydrophilic PEG-block (black). Polymeric micelles are formed by individual unimers in water. In the shell-region, a radiolabel is shown.

the in vivo stabilities of DOTA and CB-TE2A, these two chelators were attached to the micelles. By conjugating the chelators in the shell-region, we envisaged that they would be protected by the PEG-layer, thereby reducing/negating direct interaction of the chelators with blood components and possibly transchelation. The micelle core was made from a 4-methylcoumarin polymer that was cross-linked by irradiation with UV light (Figure 2), ensuring thermodynamic stability of the micelles in vivo.[31,32] To the best of our knowledge, this is

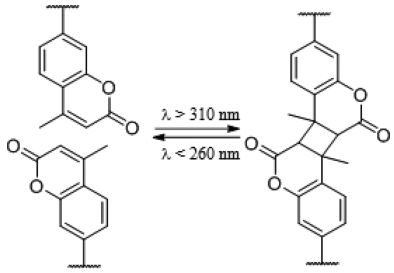

Figure 2. UV-induced cross-linking of 4-methylcoumarin moieties. Coumarin derivatives undergo 2 + 2 photodimerization to form a cyclobutane ring when exposed to UV light of λ > 310 nm. The reaction is reversed by UV light of λ < 260 nm.

the first time a cross-linked micelle has been labeled with ^{64}Cu to compare the biodistribution of different chelating agents.

MATERIALS AND METHODS

Materials. DOTA-NHS ester was purchased from CheMatech. CB-TE2A·2H_2O was purchased from Macrocyclics. All solvents and chemicals were purchased from Sigma Aldrich. CuCl (99.995%) was washed with acetic acid followed by ethanol (99%) and diethylether, dried, and stored under argon. Solvents used for ATRP were purified by distillation over $Mg(OMe)_2$ (MeOH) or CaH_2 (DMF), stored over mol. sieves (MeOH, 3 Å; DMF, 4 Å) and transferred under argon. CH_3−PEG_{5000} was from Fluka. DMF for anhydrous syntheses was dried over 4 Å molecular sieves several times. Glassware was oven dried overnight or heatgun dried under a stream of argon prior to use. Reactions other than polymerizations were conducted in a nitrogen atmosphere. Polymers and micelles containing coumarin moieties were shielded from light whenever possible. Cellulose membrane dialysis tubing (12.4 kDa cutoff) was from Sigma Aldrich.

Size-exclusion chromatography (SEC) was carried out on an automated apparatus, custom-built at out facility, using Sephadex G25 fine (GE Healthcare, fractionation range: 1000−5000 Da) as stationary phase and 10 mM PIPES buffer (pH 7.0, 150 mM NaCl) as eluent, flow rate of 0.5 mL/min, room temperature and column dimensions of 20 × 1.5 cm. NMR-analyses were recorded in $CDCl_3$ on a 300 MHz Varian Mercury 300 BB and referenced to $CHCl_3$ (δ 7.26). Photo cross-linking by UV irradiation was done on an Omnicure Series 1000 (Lumen Dynamics). FT-IR spectra were recorded by Perkin-Elmer Spectrum 100 FT-IR Spectrometer. GPC measurements were carried out with a RID10A-SHIMADZU refractive index detector and Mixed-D GPC column from Polymer Laboratories with a flow rate of 0.5 mL/min at 25 °C, and DMF with 50 mM LiCl as eluent. UV−vis spectra were recorded on a Unicam Helios Uni 4923 spectrophotometer. Size and zeta potential were measured on a ZetaPALS. ^{64}Cu was produced on a GE PETtrace Cyclotron. Radio-TLCs were analyzed on a Raytest MiniGita Star. As radio-TLC eluent was used 5% (w/v) NH_4OAc in H_2O-MeOH (1:1), R_f of ^{64}Cu-EDTA, 0.7; R_f of ^{64}Cu-DOTA, 0.4; R_f of ^{64}Cu-CB-TE2A, 0.3.

Synthesis of PEG-PHEMA-PCMA (3). The macroinitiator PEG-Br (**1**) and the diblock copolymer PEG-PHEMA-Cl (**2**) were synthesized as previously described.[33] The monomer 7-(2-methacryloyloxyethoxy)-4-methylcoumarin (CMA) was synthesized as reported by Obi et al.[34] The diblock copolymer PEG-PHEMA-Cl (1.00 g, 0.152 mmol), CMA (1.10 g, 3.80 mmol), $CuCl_2$ (18.4 mg, 0.137 mmol), and PMDETA (95 μL, 0.456 mmol) were dissolved in DMF (10 mL) and frozen in liquid nitrogen. The catalyst CuCl (15.0 mg, 0.152 mmol) was added and the reaction mixture was degassed three times by freeze−pump−thaw cycles and stirred under argon at 80 °C for 24 h. Most of the solvent was removed under vacuum. The polymer was then precipitated from methanol and dried under vacuum to yield 844 mg (47%). Subsequently, the unimers were purified by dialysis (see dialysis description below) to yield the pure unimer (**3**). ^{1}H NMR (300 MHz, $CDCl_3$): δ = 7.38−6.00 (coumarin H), 4.60−3.73 (−OCH_2CH_2O-coumarin, −OCH_2CH_2OH), 3.65 (s, −CH_2CH_2O

dx.doi.org/10.1021/bm401871w | Biomacromolecules 2014, 15, 1625−1633

of PEG), 2.30 (s, $-CH_3$ of coumarin), 2.16−1.72 ($-CH_2$ backbones of PHEMA and PCMA blocks), 1.20−0.79 ($-CH_3$ backbones of PHEMA and PCMA blocks) ppm. FTIR (cm^{-1}): 3490, 2880, 1718, 1612, 1467, 1391, 1343, 1279, 1240, 1140, 1100, 963, 839, 750. M_n (from NMR) = 11 814. From GPC: M_w = 12 400, M_n = 9550, PD (M_w/M_n) = 1.3.

Synthesis of 4 by Conjugation of DOTA. PEG-PHEMA-PCMA (30 mg, MW: 11.8 kDa, 2.5 μmol) was dissolved in dry DMF (1 mL) under a nitrogen atmosphere. DOTA-NHS ester (2.0 mg, 2.7 μmol) was added along with DMAP (2.0 mg, 16 μmol). The mixture was stirred overnight (19 h) at RT, followed by micelle formation and dialysis as described below.

Synthesis of 5 by Conjugation of CB-TE2A. In the main reaction vessel, (MRV) was dissolved PEG-PHEMA-PCMA (30 mg, MW: 11.8 kDa, 2.5 μmol) and CB-TE2A·$2H_2O$ (4.5 mg, 8.2 μmol) in dry DMF (1 mL). DMAP (17 mg) was dissolved in dry DMF (4 mL) and 40 μL of this solution was added to the MRV (DMAP added: 0.17 mg, 1.4 μmol). EDC·HCl (4.0 mg) was dissolved in dry DMF (0.5 mL) and 69 μL of this solution was added to the MRV (EDC·HCl added: 0.55 mg, 2.9 μmol). The mixture was stirred overnight (16 h) at RT under a N_2 atmosphere, followed by micelle formation and dialysis as described below.

Formation of Micelles by Dialysis. Upon chelator conjugation, Milli-Q water was added dropwise directly to the reaction mixture until the ratio of DMF-water was 1:2. The mixture was placed in a dialysis tube (cutoff: 12.4 kDa) and dialyzed against Milli-Q water (1 L) for three days at pH < 7. Each day the water was changed. Conjugation yield was estimated by incubating the micelle dispersion (200 μL, 1 equiv) with nonradioactive Cu^{2+}, twice the maximum molarity of chelator present (2 equiv), spiked with ^{64}Cu. After incubation for 4 h at 80 °C (CB-TE2A) or 3 h at room temperature (DOTA), unincorporated copper was scavenged (for 30 min) by adding EDTA in excess (400 equiv). Conjugation yield was estimated by radio-TLC and given as the ratio of the noneluting peak (micelles) to the EDTA-peak.

Characterization of Micelles. The micelles were characterized by dynamic light scattering (DLS), providing the nanoparticle hydrodynamic diameters and zeta-potential. Size was measured three times on the same sample unless otherwise stated. The number weighted median sizes are reported along with the PDI. Intensity weighted sizes are available in the Supporting Information when specified. Zeta-potentials were measured by running 20 runs of 10 scans on one sample (n = 10, unless otherwise specified). All graphs had maxima around 320 nm. At this wavelength, treatment with UV light (2 W/cm^2, 320−500 nm) for 30 min resulted in absorbance drops of 0.709 → 0.412 (42%) for DOTA and 0.664 → 0.366 (45%) for CB-TE2A.

Photo Cross-Linking of Micelles. Micelle dispersion (1100 μL) was transferred to a 4 mL glass vial containing a magnet. The vial was stirred vigorously and placed in an ice/water bath that was kept at 5−7 °C. The dispersion was irradiated for 2 × 15 min at an intensity of 2 W/cm^2 and a wavelength of 320 < λ < 500 nm. The UV probe was placed about a centimeter from the water surface. The degree of cross-linking (% CL) was determined by measuring the drop in absorbance at 320 nm and calculating $((A_{before} - A_{after})/(A_{before} - A_0)) \times 100\%$ = % CL, where A_0 was set to zero. Cross-linking was verified by mixing 100 μL of cross-linked or noncross-linked micelle dispersions with 1600 μL DMF and measuring size and count rate by DLS.

Determination of Micelle Material Concentration. Determining the concentration of micelle material in dispersion was possible since coumarin absorbs UV light. There was a direct linear correlation between amount of micelle material (determined by lyophilizing an aliquot of dispersion and weighing the dry residue) and UV absorption at 320 nm with intercept through (0,0). This made it possible to measure the absorbance of a micelle dispersion of known concentration and determining the concentration in diluted samples based on this value.

Radiolabeling with ^{64}Cu. To a vial containing $^{64}CuCl_2$ was added 100 μL NH_4OAc (0.1 M, pH 5.5) buffer. The mixture was stirred for 10 min at room temperature. Then micelle dispersion (400 μL, ∼4 mg/mL) was added. This mixture was stirred for 2 h at room temperature (DOTA) or 3 h at 80 °C (CB-TE2A). Then 1 mM EDTA-tripotassium-dihydrate (0.05 μmol, 50 μL) was added and the mixture was stirred for 20 min, concurrently cooling to room temperature (CB-TE2A). The radiolabeled micelles were applied to a fully automated size-exclusion column and eluted with an isotonic 10 mM PIPES buffer (pH 7.0, 150 mM NaCl). The activity eluted in two peaks, Peak 1 (micelles) and Peak 2 (small molecules, such as EDTA-chelated ^{64}Cu).

Formulation of Micelles for Animal Studies. From the SEC, purification of the radiolabeled micelles, the most concentrated fraction (1 mL, ∼1.0 mg/mL) from Peak 1 was used. This was diluted with nonradiolabeled, identical micelles to give final concentrations of about 1.0 mg micelle material per mL and ∼70 MBq/mL.

MicroPET/CT Imaging. Seven week old female NMRI nude mice, purchased from Tarconic, were inoculated in the right and left flank with 5 × 10^6 U87MG cells (LGC standards, Boras, Sweden) in a 1:1 mixture with matrixgel (BD Biosciences). Tumors were grown for two weeks. The mice were divided into two groups: CB-TE2A (n = 6) and DOTA (n = 6). The animal experiments were approved by the Animal Research Committee of the Danish Ministry of Justice. The micelle formulations were intravenously injected in a lateral tail vein of anesthetized mice at an average dose of 7.8 ± 0.46 MBq (mean ± SD) for the CB-TE2A micelles and 8.0 ± 0.84 MBq for the DOTA-micelles at a volume of 200 μL and a micelle material concentration of ∼1.0 mg/mL. The PET/computed tomography (CT) scans were acquired on a dedicated small animal system (MicroPET Focus 120 and MicroCAT II, Siemens Medical Solutions, Malvern, PA, U.S.A.) at 1, 22. and 46 h postinjection (p.i.) with PET acquisition times of 10, 15, and 30 min, respectively. PET data were reconstructed with the two-dimentional ordered-subset expectation maximization (OSEM2D) reconstruction algorithm. PET and CT images were analyzed as fused images using the Inveon software (Siemens) where regions of interest (ROIs) were drawn around liver, kidney, spleen, muscle, tumors, and the left-ventricle. Uptake in the left ventricle of the heart was taken as a measure of the blood concentration. CT settings were a tube voltage of 64 kVp, a tube current of 500 μA, 360 rotation steps, an exposure time of 400 ms and a voxel size of 0.092 mm. Immediately following the last PET scan, four of the six mice in each group were euthanized and blood as well as organs of interest collected and counted in a gamma counter (Perkin-Elmer Life Sciences). The statistics were calculated using Excel 2010. Differences were analyzed using an unpaired, two-tailed t-test. Differences in the same animal at different times p.i were analyzed using a paired, two-tailed t-test. A p-value <0.05 was considered significant (*). Significance levels below 0.005 is indicated by two asterisks (**) and below 0.001 with three asterisks (***). Error bars on tracer accumulation (% ID/g) are presented as standard error of the mean (SEM).

RESULTS

Synthesis and Chelator Conjugation. The amphiphilic triblock copolymer PEG-PHEMA-PCMA (**3**) was synthesized by a two-step copper-catalyzed isolated macroinitiator ATRP (Scheme 1). The copolymers were characterized by ^1H NMR and FT-IR spectroscopy (see Supporting Information). Number average molecular weight (M_n) and degree of polymerization was calculated from ^1H NMR. GPC analysis was used to calculate the molecular weights (M_w and M_n) and polydispersity (PD) of the amphiphilic triblock copolymer.

After synthesis, the PEG-PHEMA-PCMA unimer was purified by dialysis. Dialysis was necessary in order to remove small molecular contaminants and residual copper from the polymerization steps. In order to prevent the formation of the copper hydroxide, it was made sure that pH was kept below 7 during dialysis. Micelle size after dialysis: 29 ± 2 nm. PDI: 0.21 ± 0.02. Zeta potential: −4.1 ± 0.4 mV.

DOTA and CB-TE2A were conjugated to PEG-PHEMA-PCMA through ester bonds (Scheme 2). DOTA was

Scheme 1. Synthesis of PEG-PHEMA-PCMA[a]

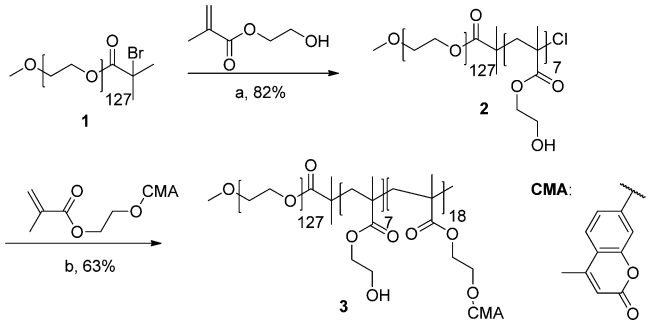

[a]Reagents and conditions: (a) CuCl/bpy, MeOH, 25 °C, 24 h, (b) CuCl/PMDETA, $CuCl_2$, DMF, 80 °C, 24 h.

conjugated by using the commercially available DOTA-NHS ester. DMAP was added in excess in order to function as both base and acyl transfer catalyst in a variation of Steglich esterification. CB-TE2A, not being available as an activated ester, was conjugated through EDC-mediated coupling, in the presence of DMAP. EDC and CB-TE2A were used in a 1:3 ratio to ensure activation of predominantly one carboxylic acid on CB-TE2A. DMAP was added as catalyst. These conjugations were low yielding possibly due to the presence of water (estimated yields: DOTA, 4%; CB-TE2A, 5%); however, as only relatively few chelators are needed in the shell-region due to the sensitivity of PET, this was not a limitation. Approximately 5% of the unimers in the micelles were conjugated with a chelator.

Micelle Preparation and Cross-Linking. After chelator conjugation was carried out, micelles were formed by dropwise addition of water directly to the reaction mixture. The mixture was subsequently dialyzed against ultrapurified water. The physicochemical properties of the prepared micelles are shown in Table 1. The micelle sizes were in the range of 31−36 nm (nr. weighted) with slightly negative zeta potentials. Chelator conjugation was not generally observed to affect the size or the zeta potentials of the micelles. The micelle material concentrations in the two formulations were measured to be 3.9 mg/mL (DOTA micelles) and 4.2 mg/mL (CB-TE2A micelles). Cross-linking was carried out by UV irradiation. We have previously observed (unpublished results) that prolonged exposure to UV without temperature control can induce instability and aggregation of certain micelle types. For this reason, cross-linking was done at low temperature (5−7 °C). In line with previous work, we observed that the rate of cross-linking decreased with exposure time.[31] As such, it became a compromise between achieving an appreciable degree of cross-linking and exposing the micelles to potentially damaging UV radiation for too long. Cross-linking rate was also found to depend on the concentration of the dispersion with more concentrated dispersions needing longer exposure to UV light. We assessed that 40−50% cross-linking was sufficient to ensure that every unimer was linked to at least one other unimer, thus ensuring continuous cross-linking of the entire micelle. This correlated with a total of 30 min of irradiation. Cross-linking degrees of 42% (DOTA) and 45% (CB-TE2A) were obtained (see Figure 3 and Table 1). In order to test the stability of cross-linked veraus noncross-linked micelles the dispersions were mixed with DMF in a 1:16 dispersion/DMF ratio. DMF is a nonselective solvent, capable of fully dissolving the micelles into single unimers. The cross-linked micelles were found to be stable when mixed with DMF. Sizes of 29 ± 3 nm (DOTA) and 34 ± 4 nm (CB-TE2A) and PDIs of 0.095 (DOTA) and 0.059 (CB-TE2A), as well as normal DLS count rates were obtained. The noncross-linked micelles all disintegrated when mixed with DMF and were nondetectable by DLS, giving count rates comparable to background scattering (<10), poorly defined sizes and PDIs of 0.398 (DOTA) and 1.190 (CB-TE2A). These results indicated that cross-linking was successful and that the cross-linked micelles were stable when exposed to DMF, whereas noncross-linked micelles were not.

Radiolabeling and Formulation. Both cross-linked and noncross-linked micelles were radiolabeled with ^{64}Cu, despite only the cross-linked micelles being used *in vivo*. Initially it was

Scheme 2. Conjugation of Chelators to PEG-PHEMA-PCMA[a]

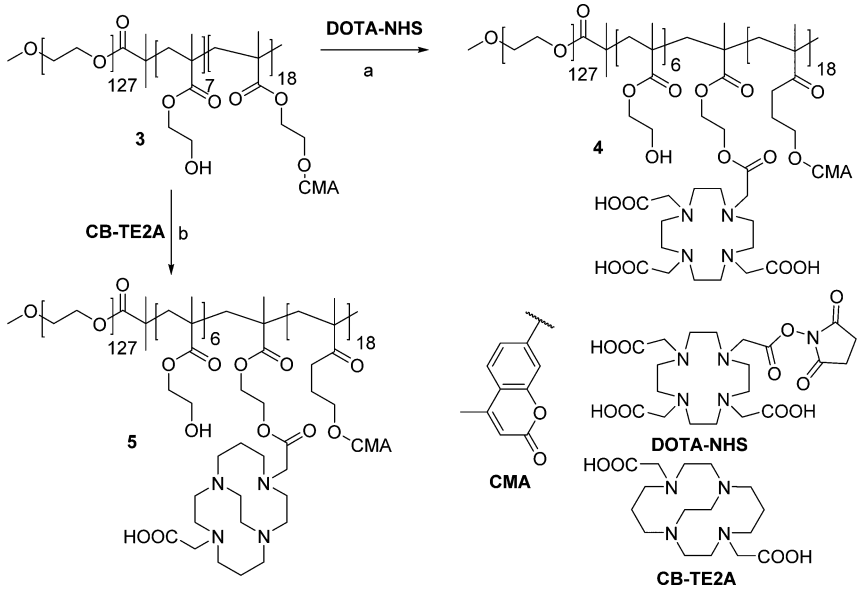

[a]Reagents and conditions: (a) DMAP, DMF, 19 h, RT. (b) EDC·HCl, DMAP, DMF, 16 h, RT.

Table 1. Physiochemial Properties of Micelle Formulations[a]

	CB-TE2A (CL)	DOTA (CL)	CB-TE2A (NonCL)	DOTA (NonCL)
size (nr. weighted)	36 ± 2 nm	33 ± 3 nm	36 ± 3 nm	31 ± 5 nm
PDI	0.04 ± 0.01	0.06 ± 0.03	0.04 ± 0.01	0.06 ± 0.03
zeta-pot.	−3.5 ± 0.3 mV	−2.3 ± 0.4 mV	−3.8 ± 0.4 mV	−2.1 ± 0.7 mV
cross-linking	45%	42%	NA	NA
labeling efficiency	47% (30%)	60% (34%)	40% (23%)	76% (50%)
mic. mat. conc.	1.1 mg/mL	0.9 mg/mL	NA	NA

[a]The labeling efficiency is the percent of the total activity in Peak 1. The contents of the pooled fractions that were used in the in vivo study are given in parentheses. Mic. mat. conc. denotes micelle material concentration. CL, cross-linked; NonCL, noncross-linked. n = 3 in all cases, except zeta potential (n = 10). For intensity weighted sizes, see Supporting Information.

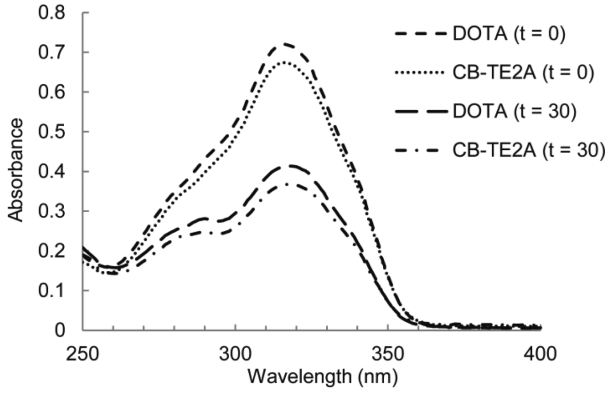

Figure 3. UV chromatograms of micelles before and after cross-linking. All graphs had maxima around 320 nm. At this wavelength, treatment with UV light (2 W/cm^2, 320−500 nm) for 30 min results in a drop in absorbance, 0.709 → 0.412 (42%) for DOTA and 0.664 → 0.366 (45%) for CB-TE2A.

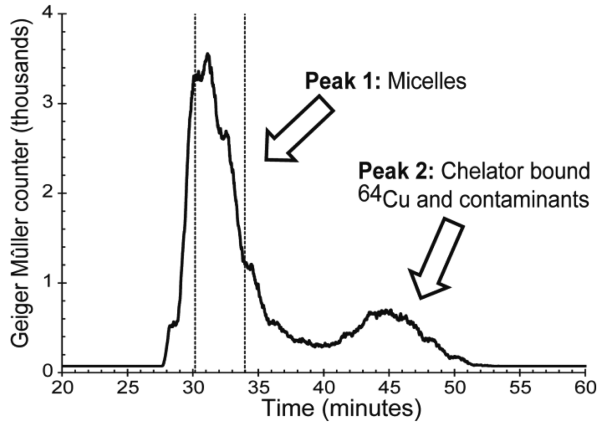

Figure 4. SEC of the purification of the radiolabeled micelles. Peak 1: ^{64}Cu bound to micelles. Peak 2: ^{64}Cu bound to free chelator (especially EDTA) and small-molecular contaminants. The concentrated fractions (1 mL total) between the two dotted lines were formulated for in vivo use. The data shown are for DOTA micelles. Conditions: Sephadex G25 fine as stationary phase, 10 mM PIPES buffer (pH 7.0, 150 mM NaCl) as eluent, flow rate, 0.5 mL/min, room temperature, column dimensions, 20 × 1.5 cm.

attempted to label the CB-TE2A micelles at 95 °C, but this caused them to aggregate. Three hours at 80 °C (pH 5.5) provided good labeling efficiency and this was chosen as the standard procedure. Similar conditions were used by Seo et al. for labeling CB-TE2A on the surface of liposomes with ^{64}Cu.[26] Nonspecifically bound ^{64}Cu was removed by EDTA scavenging (50 μmol, 20 min incubation). ^{64}Cu that is nonspecifically bound to tracers such as micelles can potentially disturb PET imaging analysis by accumulating in other organs than the micelles. When micelles with no conjugated chelator were incubated with ^{64}Cu for 2 h at room temperature under conditions similar to radiolabeling conditions 7% of the activity eluted with the micelles on SEC. EDTA scavenging for 20 min lowered this to 2%. Accordingly, $^{64}Cu^{2+}$ showed little tendency to bind nonspecifically to these micelles. However, when micelles with no conjugated chelator were incubated with ^{64}Cu for three hours at 80 °C (CB-TE2A labeling conditions) Seventeen percent of the activity became nonspecifically bound. Subjecting to EDTA challenge for 20 min lowered this to 8%. It is reasonable to assume that nonspecific binding is even lower in the presence of conjugated chelators due to the shift of ^{64}Cu to such chelators during incubation. Accordingly, nonspecific binding of ^{64}Cu to these micelles is not considered to influence biodistribution analysis significantly.

The radiolabeled micelles were purified by size-exclusion chromatography, resulting in two peaks (Figure 4). It was confirmed that Peak 1 contained micelles where the radioactivity correlated with count rate on DLS as well as the intensity of the absorbance of coumarin units. Peak 1 was routinely analyzed by radio-TLC showing a single peak that did not elute, which is characteristic for this type of nanoparticles. Analysis of Peak 2 by radio-TLC usually showed a prominent peak for ^{64}Cu-EDTA as well as small molecular contaminants. Radiolabeling efficiencies are seen in Table 1. Generally, DOTA micelles were labeled with higher efficiencies than CB-TE2A micelles.

The most concentrated fraction (in total 1 mL) of Peak 1 was collected. The concentration of radiolabeled micelles was ∼1.0 mg/mL micelle material, which was determined by UV measurements after radioactivity had decayed. For the final formulation for the in vivo studies, the radioactive micelles were diluted with a dispersion of nonradioactive micelles, also prepared in isotonic PIPES buffer and also having a concentration of ∼1.0 mg/mL. The final concentrations of the formulations used for in vivo studies was 1.1 mg/mL for CB-TE2A micelles and 0.9 mg/mL for DOTA micelles. With 200 μL injected into each mouse, this gave a dose per mouse of 0.2 mg or ∼8 mg/kg. When nanoparticles are administered, a dose-dependent proportion is sequestered by the RES immediately after injection.[35,36] For this reason, it is necessary to inject an appreciable amount of micelle material, as trace amounts would be rapidly cleared. For lipid nanoparticles (liposomes), the lower limit of dose-independent pharmacokinetics has been reported to be about 2 μmol/kg (∼2 mg/kg).[35] In previous studies with polymeric micelles in mice, 3−5 mg/kg[37,38] and 10 mg/kg[5,39] have been used. This suggests that 8 mg/kg is within the window of dose independent pharmacokinetics.

dx.doi.org/10.1021/bm401871w | Biomacromolecules 2014, 15, 1625−1633

Stability of the Micelles. The size stability of the cross-linked micelles was investigated by DLS at 37 °C (physiological temperature) and 80 °C (radiolabeling temperature). At 37 °C, both DOTA and CB-TE2A micelles were found to be stable for up to 6 days (no further measurements) as no changes in size were seen. At 80 °C, the DOTA-micelles were stable up to 61 h (no further measurements). The CB-TE2A micelles were stable with no size change up to 4.5 h. Beyond 4.5 h, however, this micelle type aggregated at 80 °C. We concluded that the micelles were stable during the labeling procedure and the in vivo studies.

In order to investigate whether the labeling process itself, especially the exposure to high radioactivity, compromised micelle stability, the radiolabeled micelle dispersions were stored for one week, after which the micelles were analyzed by DLS. The sizes and zeta-potentials obtained after radiolabeling were for the CB-TE2A micelles 29 ± 1 nm, PDI, 0.08, zeta potential, −1.1 ± 0.6 mV. For the DOTA micelles, the values after radiolabeling were 34 ± 0 nm, PDI, 0.05, zeta potential, −2.1 ± 1.3 mV. By comparing with the values before radiolabeling (Table 1) we could conclude that the micelles had not significantly changed size or charge.

In Vivo PET and Biodistribution. Using PET and CT the tumor volume as well as the in vivo biodistribution of the ^{64}Cu-labeled CB-TE2A and DOTA micelles were evaluated in mice bearing subcutaneously inoculated U87MG tumors on the right and left flank. The tumor volume was assessed on every CT scan and found to be 56.7 ± 11.8 mm^3 (n = 12) and 56.8 ± 10.6 mm^3 (n = 12) in the CB-TE2A and the DOTA groups, respectively. Tumor uptake, organ distribution, and plasma stability were evaluated over a 46 h time frame with PET/CT scans at 1, 22, and 46 h p.i., as well as radioactivity measurements at 48 h p.i. using a gamma counter.

The circulation time of both micelle types was found to be relatively long with blood values of 21.7 ± 1.7% ID/g (1 h) and 4.7 ± 0.30% ID/g (46 h) for the CB-TE2A micelles and 15.9 ± 0.74% ID/g (1 h) and 2.7 ± 0.18% ID/g (46 h) for the DOTA micelles. All blood values for CB-TE2A were slightly higher than for DOTA. In agreement with the EPR-effect and plasma stability of the two micelle formulations, the tumor accumulation increased over time and was significantly higher at the 22 and 46 h time-points compared to the 1 h time-point for both groups (p < 0.001 in all cases). In addition, for the CB-TE2A micelles there was a significant increase in tumor accumulation from 4.0 ± 0.35% ID/g at 22h p.i. to 4.9 ± 0.43% ID/g at 46h p.i. (p < 0.001). In contrast, there was a significant decrease in tumor retention from 3.8 ± 0.13% ID/g at 22 h p.i. of the DOTA micelles compared to 3.6 ± 0.11% ID/g at 46 h p.i. (p = 0.029) (Figure 5). Between the two chelator groups there was a significantly higher tumor uptake at 46 h p.i. in the CB-TE2A group compared to the DOTA group (p = 0.0083) whereas there was no significant difference between the two groups at 1 and 22 h p.i.. Accumulation in liver and spleen were modest for both micelle types (peak values at 1 h being about 5−8% ID/g in all cases), and slightly higher for CB-TE2A. For both organs, accumulation was highest initially (1 h) followed by slow elimination. This pattern was also seen for the kidneys but, as mentioned, not for the tumors. All organ values, as well as ex vivo results from gamma counting of excised organs, and calculated organ ratios are shown in Table 2.

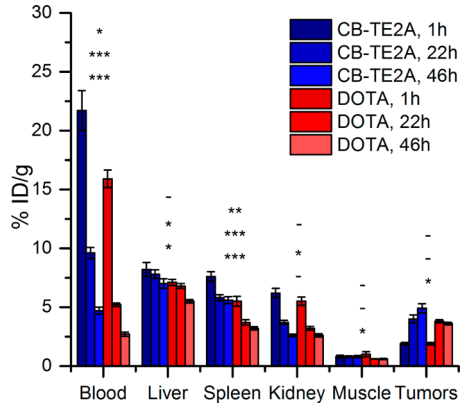

Figure 5. In vivo distribution of DOTA and CB-TE2A conjugated micelles. PET scans were conducted after 1, 22, and 46 h. Organ accumulation was quantified by region-of-interest (ROI) image analysis. Differences between the two chelators were analyzed using a paired two-tailed t-test. Significance is shown for each organ as not significant (−), p < 0.05 (*), p < 0.01 (**), or p < 0.001 (***) with the top symbol representing t = 1 h, the middle t = 22 h, and the bottom t = 46 h. All values are ±SEM with n = 6, except for tumors where n = 12.

DISCUSSION

In this study, we prepared triblock polymeric micelles conjugated with CB-TE2A or DOTA in the micelle shell-region and radiolabeled these with ^{64}Cu in good yields. The micelles were cross-linked by UV radiation to ensure micelle integrity in vivo. As these micelles were cross-linked, it was crucial to show that they maintained integrity when faced with conditions that would cause regular micelles to dissolve. It was attempted to investigate the critical micelle concentration (CMC) of cross-linked versus noncross-linked micelles by the pyrene assay, which takes advantage of a change in the emission spectrum of pyrene when incorporated in a nonpolar environment.[40] However, the inherent absorbance and fluorescence of the coumarin moieties made this impossible. Instead, micelles were dissolved in DMF/water (1:16) to show enhanced integrity of cross-linked micelles. In this environment, noncross-linked micelles dissolved and were undetectable by DLS, whereas UV-treated cross-linked-micelles retained their integrity.

A main objective of this study was to show whether the reported in vivo instability of DOTA has practical significance for PET imaging when compared with CB-TE2A, which is argued to be a more stable copper chelator. Both DOTA[41,42] and CB-TE2A[22,26] are commercially available and have been reported to furnish chelates with ^{64}Cu^{2+} that show excellent stability under in vitro physiological conditions, notably in serum. Therefore, this study focused on comparing their stabilities and imaging capabilities in an in vivo setting. Chelates with ^{64}Cu^{2+} are known to undergo fast renal excretion for both DOTA[18,43] and CB-TE2A,[18,44] where almost all activity is rapidly eliminated, except for DOTA where a small amount (1.05% ID/g in mice) locates to the liver through trans-chelation.[18] Therefore, to obtain prolonged circulation of the chelates it is necessary to conjugate these to long-circulating structures, such as polymeric micelles.

The in vivo studies allowed us to evaluate micelle blood circulation half-life. By assuming 2 mL (2 g) blood in a mouse, the total activity (% ID) in the blood can be plotted as shown in Figure 6. Nanoparticles generally follow a biphasic clearance

Table 2. Tissue Accumulation Values Based on PET and Ex Vivo Organ Counting[a]

	time after intravenous administration							
	1 h		22 h		46 h		ex vivo organ counting	
	CB-TE2A	DOTA	CB-TE2A	DOTA	CB-TE2A.	DOTA	CB-TE2A	DOTA
blood	21.7 ± 1.7	15.9 ± 0.74	9.6 ± 0.47	5.2 ± 0.14	4.7 ± 0.30	2.7 ± 0.18	3.4 ± 0.27	1.8 ± 0.09
liver	8.2 ± 0.6	7.1 ± 0.25	7.8 ± 0.36	6.8 ± 0.21	7.0 ± 0.40	5.5 ± 0.14	4.7 ± 0.09	3.7 ± 0.26
spleen	7.6 ± 0.4	5.5 ± 0.43	5.8 ± 0.26	3.7 ± 0.22	5.6 ± 0.30	3.2 ± 0.14	6.0 ± 0.43	3.4 ± 0.22
kidney	6.2 ± 0.4	5.5 ± 0.35	3.7 ± 0.18	3.2 ± 0.15	2.6 ± 0.10	2.6 ± 0.14	1.9 ± 0.14	2.6 ± 0.15
muscle	1.0 ± 0.11	1.0 ± 0.22	0.8 ± 0.06	0.6 ± 0.01	0.8 ± 0.1	0.6 ± 0.05	0.3 ± 0.04	0.3 ± 0.04
tumors	1.9 ± 0.10	1.9 ± 0.10	4.0 ± 0.35	3.8 ± 0.13	4.9 ± 0.40	3.6 ± 0.11	4.0 ± 0.28	3.4 ± 0.19
T/B	0.1 ± 0.01	0.1 ± 0.00	0.4 ± 0.02	0.7 ± 0.04	1.0 ± 0.08	1.4 ± 0.08		
T/M	2.0 ± 0.24	3.0 ± 1.09	5.0 ± 0.23	6.2 ± 0.26	6.3 ± 0.65	6.3 ± 0.61		
T/L	0.2 ± 0.02	0.3 ± 0.01	0.5 ± 0.02	0.6 ± 0.01	0.7 ± 0.04	0.7 ± 0.02		
T/S	0.3 ± 0.02	0.4 ± 0.02	0.7 ± 0.03	1.0 ± 0.05	0.9 ± 0.06	1.1 ± 0.04		
heart							1.2 ± 0.10	1.4 ± 0.06
lung							2.1 ± 0.13	2.0 ± 0.17
intestine							1.1 ± 0.07	1.7 ± 0.13
pancreas							0.8 ± 0.12	0.7 ± 0.06

[a]Values are represented as %ID/g, mean ± SEM. For the PET scans $n = 6$ in all cases, except tumors where $n = 12$. For the gamma counting, $n = 4$ in all cases, except tumors and kidneys where $n = 8$. The ex vivo gamma counting was performed at 48 h, after PET scans had been completed. T/B: tumor-to-blood ratio. T/M: tumor-to-muscle ratio. T/L: tumor-to-liver ratio. T/S: tumor-to-spleen ratio.

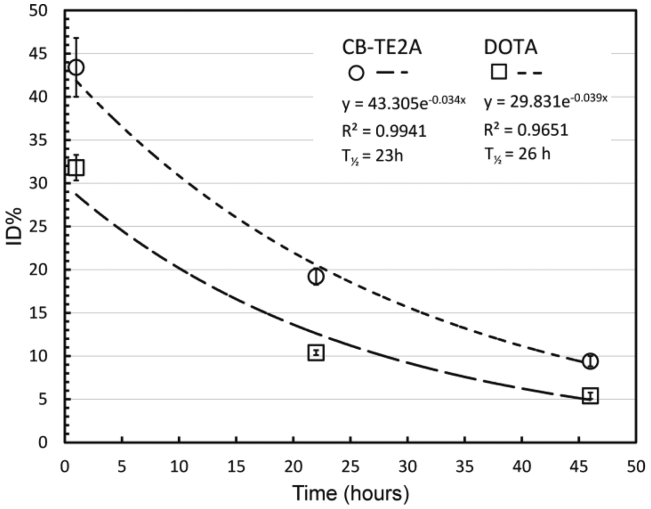

Figure 6. Blood clearance data for DOTA and CB-TE2A conjugated micelles. Values are given as % ID, assuming 2 mL blood per mouse. Equations, correlation factors (R^2), as well as calculated half-lives are shown.

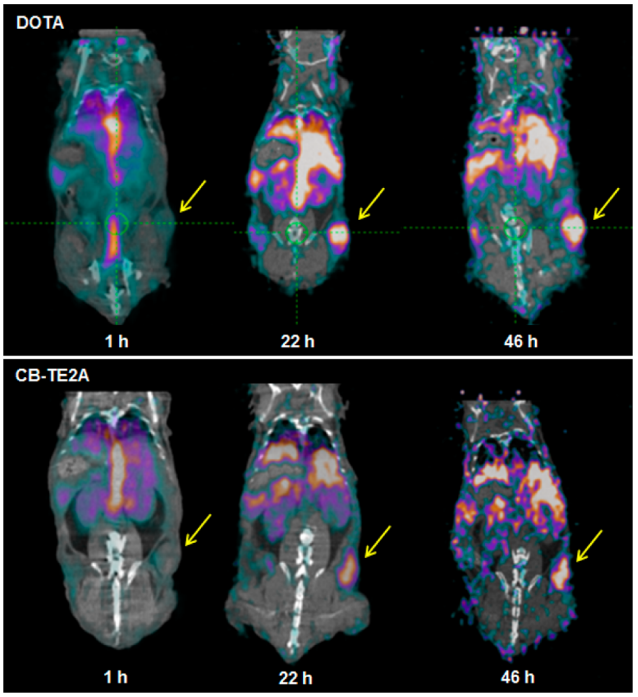

Figure 7. Example of fused PET/CT images of the DOTA (upper panel) and CB-TE2A (lower panel) conjugated micelles in mice with U87MG tumor xenograft (tumor in right flank on displayed slices, marked with an arrow). The images reveal the biodistribution at 1, 22, and 46 h postinjection with good tumor accumulation and modest uptake in liver and spleen for both chelators.

profile[8,45,46] with a fast initial clearance (usually within the first 1−2 h) followed by a longer main clearance phase where most nanoparticles have a blood half-life in mice of 6−24 h, depending on the particle type.

The initial (1 h) blood concentration is relatively low for both DOTA and CB-TE2A micelles showing that a fast initial clearance is occurring for these micelles, at least in the injection concentration used. The initial DOTA micelle clearance was found to be higher than that of the CB-TE2A micelles. PET images from other sections on which the bladder is clearly seen (see Supporting Information) show that considerable renal filtration has taken place. This may have been a primary contributor to the substantial initial clearance but due to bladder emptying, quantification was not feasible. Initial bladder accumulation is not uncommon for polymeric micelles and small nanoparticles in general. This initial clearance seems to be higher for the DOTA micelles. It should be noted that the sizes of the two types of micelles were similar and both were above the renal clearance threshold normally considered to be about 10 nm. However, the micelles are probably soft and deformable and the smallest particles within the distribution may be cleared through the kidneys. It is possible that the difference in initial clearance is due to normal variation with resulting lower accumulation for the DOTA micelles in almost all other organs. Another reason for lower initial concentrations of the DOTA micelles could be clearance by the immune system, but there is

dx.doi.org/10.1021/bm401871w | Biomacromolecules 2014, 15, 1625−1633

no indication of a faster immune response mediated clearance of the DOTA micelles. This would normally result in high uptake in macrophage-rich tissues, in particular liver and spleen. If the clearance was due to rapid loss of ^{64}Cu from the micelles, this activity would be expected to show rapid (within 1 h) and substantial accumulation, primarily in the liver[47] and the kidneys.[48] Some activity could later reappear in the blood as a protein bound fraction.[47,49] In addition, free ^{64}Cu has been shown to accumulate in tumors but not in the spleen.[50] We did observe substantial splenic accumulation and we did not find accumulation in liver and kidneys corresponding to the observed initial elimination. Therefore, it seems that after the initial clearance, the micelles follow general nanoparticle pharmacokinetics with expected tissue distribution and that there is no or little tendency for Cu^{2+} dissociation, both from nonspecifically bound ^{64}Cu or due to chelator instability. As shown in Figure 6 the circulation half-lives of the two micelles are similar after the first clearance with a circulation half-life of 26 and 23 h for DOTA and CB-TE2A micelles, respectively. Polymeric micelles usually exhibit longer biological half-lives than liposomes. Accordingly, the half-lives we observed were generally longer than those observed for liposomes where we have previously found half-lives of around 8−10 h,[43,46] while similar values, and longer, have been observed for other polymeric micelles.[27,45,51] Liposomes often accumulate in the spleen about 3−4 times as much as we observed here.[43,46] Liver accumulation of liposomes is usually more modest and is generally similar to what we observe here[43,52] or slightly higher.[46] Decreased hepatic and splenic accumulation of polymeric micelles may be related to the smaller size of the micelles in comparison to liposomes that are in the 100−130 nm size range in most studies.

Contrary to the other organs, tumor values between the two types of micelles are very similar at 1 and 22 h (Table 2). At 46 h, however, the CB-TE2A micelle concentration is higher than for DOTA micelles. As all other tissues exhibit lower values for DOTA than for CB-TE2A micelles in Figure 5, it seems reasonable to conclude that the two micelle systems have very similar tumor accumulation properties. The tumor accumulation values (4−5% ID/g) observed here fit well with generally observed accumulation for long-circulating nanoparticles. Both lower[12,27] and higher[37,45,51] values have been reported in the literature and it is generally accepted that this is xenograft model dependent. We conclude that the tumor accumulation was similar to that found for other nanoparticles, such as liposomes, and we find the accumulation in liver and spleen to be modest. Tumor-to-muscle (T/M) ratios obtained were relatively high, reaching slightly above 6 for both micelle types (Table 2). This attests to the preferential accumulation of these micelles in tumor tissue. In order to visualize pathological foci in the body, T/M ratios above 1.5 are needed.[53] Both micelle formulations investigated in the present study had T/M ratios above 6 at 46 h and can thereby provide good tumor visualization. Also, the tumor-to-blood (T/B) ratio increases for the nanoparticles, which shows that there is an accumulation effect of the micelles over time. The tumor-to-liver (T/L) and tumor-to-spleen (T/S) ratios are indicative of the nanoparticles' tendency to accumulate in tumors relative to the main nanoparticle clearance organs. These values are (as already alluded to above) generally good for these PMs. At 46 h, the T/L ratios for both micelle types are at 0.7 with T/S ratios of ∼1.

CONCLUSIONS

We prepared DOTA or CB-TE2A conjugated triblock polymeric micelles to study the radiolabeling performance of these two chelators for ^{64}Cu in vivo and the biodistribution of this class of micelles. The micelles displayed long circulation half-life in blood and good tumor accumulation with modest uptake in liver, spleen, and other organs. On the basis of this study, we do not find sufficient evidence for concluding that CB-TE2A is a better chelator of ^{64}Cu in vivo and both chelators seem to be useful for labeling of nanoparticles. However, the high initial clearance observed relative to what we have found for ^{64}Cu labeled liposomes should be investigated further. DOTA is a very practical chelator, being widely available as a bifunctional chelator for easy conjugation. It is furthermore easy to radiolabel at ambient temperature with short incubation times. Our data indicates that it may be premature to discard DOTA as a widely used chelator because of stability issues. This was an unexpected result for us. It is also noteworthy that we did not find the tumor accumulation to be higher for the small micelles in comparison to previously studied liposomes of 100 nm in the same tumor models. This is in contrast to the growing number of articles describing that nanoparticles of 20−40 nm accumulates in tumors to a higher degree than larger nanoparticles due to higher tumor penetration.

ASSOCIATED CONTENT

Supporting Information

Supplementary PET images, NMR and IR spectra, and table with intensity weighted sizes included. This material is available free of charge via the Internet at http://pubs.acs.org.

AUTHOR INFORMATION

Corresponding Author

*E-mail: thomas.andresen@nanotech.dtu.dk. Telephone: +45 45 25 81 68. Fax: +45 45 88 77 62.

Notes

The authors declare no competing financial interest.

ACKNOWLEDGMENTS

The authors thank the staff at the Hevesy Laboratory (DTU Nutech) and CBIO (DTU Nanotech) for their fruitful discussions and daily assistance. In particular Dr. Dennis Elema, as well as Cristine Søgaard and Anette Holst for providing ^{64}Cu.

ABBREVIATIONS

ATRP, atomic transfer radical polymerization; CB-TE2A, cross-bridged 2,2′-(1,4,8,11-tetraazabicyclo[6.6.2]hexadecane-4,11-diyl)diacetic acid; CT, X-ray computed tomography; DMAP, 4-dimethylaminopyridine; DOTA, 1,4,7,10-tetraazacyclododecane-1,4,7,10-tetraacetic acid; EDC, 1-ethyl-3-(3-dimethylaminopropyl)carbodiimide; NHS, *N*-hydroxysuccinimide; NMRI, Naval Medical Research Institute; PCMA, poly(4-methylcoumarin methacrylate); PDI, polydispersity index; PET, positron emission tomography; PHEMA, poly(2-hydroxyethyl methacrylate); PIPES, piperazine-*N*,*N*′-bis(2-ethanesulfonic acid); PM, polymeric micelles; PMDETA, *N*,*N*,*N*′,*N*′,*N*″-pentamethyldiethylenetriamine; SEC, size-exclusion chromatography; SEM, standard error of the mean; SPECT, single-photon emission computed tomography; TETA, 1,4,8,11-tetraazacyclotetradecane-1,4,8,11-tetraacetic acid

REFERENCES

(1) Maeda, H. *Adv. Enzyme Regul.* **2001**, *41*, 189−207.
(2) Minchinton, A. I.; Tannock, I. F. *Nat. Rev. Cancer* **2006**, *6*, 583−592.
(3) Fang, J.; Nakamura, H.; Maeda, H. *Adv. Drug Delivery Rev.* **2011**, *63*, 136−151.
(4) Waite, C. L.; Roth, C. M. *Crit. Rev. Bioeng.* **2012**, *40*, 21−41.
(5) Cabral, H.; Matsumoto, Y.; Mizuno, K.; Chen, Q.; Murakami, M.; Kimura, M.; Terada, Y.; Kano, M. R.; Miyazono, K.; Uesaka, M.; Nishiyama, N.; Kataoka, K. *Nat. Nanotechnol.* **2011**, *6*, 815−823.
(6) Dreher, M. R.; Liu, W. G.; Michelich, C. R.; Dewhirst, M. W.; Yuan, F.; Chilkoti, A. *J. Natl. Cancer Inst.* **2006**, *98*, 335−344.
(7) Jain, R. K.; Stylianopoulos, T. *Nat. Rev. Clin. Oncol.* **2010**, *7*, 653−664.
(8) Dong, H.; Dube, N.; Shu, J. Y.; Seo, J. W.; Mahakian, L. M.; Ferrara, K. W.; Xu, T. *ACS Nano* **2012**, *6*, 5320−5329.
(9) Rahmim, A.; Zaidi, H. *Nucl. Med. Commun.* **2008**, *29*, 193−207.
(10) Willmann, J. K.; van Bruggen, N.; Dinkelborg, L. M.; Gambhir, S. S. *Nat. Rev. Drug Discovery* **2008**, *7*, 591−607.
(11) Zeng, D.; Lee, N. S.; Liu, Y.; Zhou, D.; Dence, C. S.; Wooley, K. L.; Katzenellenbogen, J. A.; Welch, M. J. *ACS Nano* **2012**, *6*, 5209−5219.
(12) Xiao, Y. L.; Hong, H.; Javadi, A.; Engle, J. W.; Xu, W. J.; Yang, Y. A.; Zhang, Y.; Barnhart, T. E.; Cai, W. B.; Gong, S. Q. *Biomaterials* **2012**, *33*, 3071−3082.
(13) Wadas, T. J.; Anderson, C. J. *Nat. Protoc.* **2006**, *1*, 3062−3068.
(14) Jones-Wilson, T. M.; Deal, K. A.; Anderson, C. J.; McCarthy, D. W.; Kovacs, Z.; Motekaitis, R. J.; Sherry, A. D.; Martell, A. E.; Welch, M. J. *Nucl. Med. Biol.* **1998**, *25*, 523−530.
(15) Anderson, C. J.; Ferdani, R. *Cancer Biother. Radiopharm.* **2009**, *24*, 379−393.
(16) Bartholoma, M. D. *Inorg. Chim. Acta* **2012**, *389*, 36−51.
(17) Bass, L. A.; Wang, M.; Welch, M. J.; Anderson, C. J. *Bioconjugate Chem.* **2000**, *11*, 527−532.
(18) Boswell, C. A.; Sun, X. K.; Niu, W. J.; Weisman, G. R.; Wong, E. H.; Rheingold, A. L.; Anderson, C. J. *J. Med. Chem.* **2004**, *47*, 1465−1474.
(19) Rogers, B. E.; Anderson, C. J.; Connett, J. M.; Guo, L. W.; Edwards, W. B.; Sherman, E. L. C.; Zinn, K. R.; Welch, M. J. *Bioconjugate Chem.* **1996**, *7*, 511−522.
(20) McQuade, P.; Miao, Y. B.; Yoo, J.; Quinn, T. P.; Welch, M. J.; Lewis, J. S. *J. Med. Chem.* **2005**, *48*, 2985−2992.
(21) Pfeifer, A.; Knigge, U.; Mortensen, J.; Oturai, P.; Berthelsen, A. K.; Loft, A.; Binderup, T.; Rasmussen, P.; Elema, D.; Klausen, T. L.; Holm, S.; von, B. E.; Hojgaard, L.; Kjaer, A. *J. Nucl. Med.* **2012**, *53*, 1207−1215.
(22) Boswell, C. A.; Regino, C. A. S.; Baidoo, K. E.; Wong, K. J.; Bumb, A.; Xu, H.; Milenic, D. E.; Kelley, J. A.; Lai, C. C.; Brechbiel, M. W. *Bioconjugate Chem.* **2008**, *19*, 1476−1484.
(23) Garrison, J. C.; Rold, T. L.; Sieckman, G. L.; Figueroa, S. D.; Volkert, W. A.; Jurisson, S. S.; Hoffman, T. J. *J. Nucl. Med.* **2007**, *48*, 1327−1337.
(24) Woodin, K. S.; Heroux, K. J.; Boswell, C. A.; Wong, E. H.; Weisman, G. R.; Niu, W. J.; Tomellini, S. A.; Anderson, C. J.; Zakharov, L. N.; Rheingold, A. L. *Eur. J. Inorg. Chem.* **2005**, 4829−4833.
(25) Sprague, J. E.; Kitaura, H.; Zou, W.; Ye, Y. P.; Achilefu, S.; Weilbaecher, K. N.; Teitelbaum, S. L.; Anderson, C. J. *J. Nucl. Med.* **2007**, *48*, 311−318.
(26) Seo, J. W.; Mahakian, L. M.; Kheirolomoom, A.; Zhang, H.; Meares, C. F.; Ferdani, R.; Anderson, C. J.; Ferrara, K. W. *Bioconjugate Chem.* **2010**, *21*, 1206−1215.
(27) Fonge, H.; Huang, H.; Scollard, D.; Reilly, R. M.; Allen, C. *J. Controlled Release* **2012**, *157*, 366−74.
(28) Ekblad, T.; Orlova, A.; Feldwisch, J.; Wennborg, A.; Karlstrom, A. E.; Tolmachev, V. *Bioorg. Med. Chem. Lett.* **2009**, *19*, 3912−3914.
(29) Sabbah, E. N.; Kadouche, J.; Ellison, D.; Finucane, C.; Decaudin, D.; Mather, S. J. *Nucl. Med. Biol.* **2007**, *34*, 293−304.
(30) Tolmachev, V.; Wallberg, H.; Andersson, K.; Wennborg, A.; Lundqvist, H.; Orlova, A. *Eur. J. Nucl. Med. Mol. Imaging* **2009**, *36*, 1460−1468.
(31) Jiang, J. Q.; Qi, B.; Lepage, M.; Zhao, Y. *Macromolecules* **2007**, *40*, 790−792.
(32) Jin, Q.; Liu, X. S.; Liu, G. Y.; Ji, J. *Polymer* **2010**, *51*, 1311−1319.
(33) Pramod Kumar, E. K.; Almdal, K.; Andresen, T. L. *Chem. Commun.* **2012**, *48*, 4776−4778.
(34) Obi, M.; Morino, S. y.; Ichimura, K. *Chem. Mater.* **1999**, *11*, 656−664.
(35) Utkhede, D. R.; Tilcock, C. P. *J. Liposome Res.* **1998**, *8*, 381−390.
(36) Laverman, P.; Brouwers, A. H.; Dams, E. T. M.; Oyen, W. J. G.; Storm, G.; Van Rooijen, N.; Corstens, F. H. M.; Boerman, O. C. *J. Pharmacol. Exp. Ther.* **2000**, *293*, 996−1001.
(37) Rossin, R.; Pan, D. P. J.; Qi, K.; Turner, J. L.; Sun, X. K.; Wooley, K. L.; Welch, M. J. *J. Nucl. Med.* **2005**, *46*, 1210−1218.
(38) Sun, X. K.; Rossin, R.; Turner, J. L.; Becker, M. L.; Joralemon, M. J.; Welch, M. J.; Wooley, K. L. *Biomacromolecules* **2005**, *6*, 2541−2554.
(39) Bae, Y.; Nishiyama, N.; Fukushima, S.; Koyama, H.; Yasuhiro, M.; Kataoka, K. *Bioconjugate Chem.* **2005**, *16*, 122−130.
(40) Wilhelm, M.; Zhao, C. L.; Wang, Y. C.; Xu, R. L.; Winnik, M. A.; Mura, J. L.; Riess, G.; Croucher, M. D.; et al. *Macromolecules* **1991**, *24*, 1033−1040.
(41) Kang, C. M.; Koo, H.-J.; Lee, K. C.; Choe, Y. S.; Choi, J. Y.; Lee, K. H.; Kim, B. T. *Biomaterials* **2013**, *34*, 6839−6845.
(42) Hanaoka, H.; Tominaga, H.; Yamada, K.; Paudyal, P.; Iida, Y.; Watanabe, S.; Paudyal, B.; Higuchi, T.; Oriuchi, N.; Endo, K. *Ann. Nucl. Med.* **2009**, *23*, 559−567.
(43) Petersen, A. L.; Binderup, T.; Rasmussen, P.; Henriksen, J. R.; Elema, D. R.; Kjaer, A.; Andresen, T. L. *Biomaterials* **2011**, *32*, 2334−41.
(44) Sun, X.; Wuest, M.; Weisman, G. R.; Wong, E. H.; Reed, D. P.; Boswell, A.; Motekaitis, R.; Martell, A. E.; Welch, M. J.; Anderson, C. J. *J. Med. Chem.* **2002**, *45*, 469−477.
(45) Zhao, J.; Song, S. L.; Zhong, M.; Li, C. *ACS Macro Lett.* **2011**, *1*, 150−153.
(46) Petersen, A. L.; Binderup, T.; Jolck, R. I.; Rasmussen, P.; Henriksen, J. R.; Pfeifer, A. K.; Kjaer, A.; Andresen, T. L. *J. Controlled Release* **2012**, *160*, 254−263.
(47) Tao, T. Y.; Gitlin, J. D. *Hepatology* **2003**, *37*, 1241−7.
(48) Di Bartolo, N. M.; Sargeson, A. M.; Donlevy, T. M.; Smith, S. V. *J. Chem. Soc., Dalton Trans.* **2001**, 2303−2309.
(49) Linder, M. C.; HazeghAzam, M. *Am. J. Clin. Nutr.* **1996**, *63*, S797−S811.
(50) Jorgensen, J. T.; Persson, M.; Madsen, J.; Kjaer, A. *Nucl. Med. Biol.* **2013**, *40*, 345−350.
(51) Hoang, B.; Lee, H.; Reilly, R. M.; Allen, C. *Mol. Pharmaceutics* **2009**, *6*, 581−92.
(52) Seo, J. W.; Zhang, H.; Kukis, D. L.; Meares, C. F.; Ferrara, K. W. *Bioconjugate Chem.* **2008**, *19*, 2577−2584.
(53) Phillips, W. T. *Adv. Drug Delivery Rev.* **1999**, *37*, 13−32.